

Physical properties of the WASP-44 planetary system from simultaneous multi-colour photometry

L. Mancini,¹* N. Nikolov,¹ J. Southworth,² G. Chen,^{1,3} J. J. Fortney,⁴ J. Tregloan-Reed,² S. Ciceri,¹ R. van Boekel,¹ and Th. Henning¹

¹Max Planck Institute for Astronomy, Königstuhl 17, 69117 – Heidelberg, Germany

²Astrophysics Group, Keele University, Newcastle-under-Lyme, ST5 5BG, UK

³Purple Mountain Observatory & Key Laboratory for Radio Astronomy, 2 West Beijing Road, Nanjing 210008, China

⁴Department of Astronomy & Astrophysics, University of California, Santa Cruz, CA 95064, USA

Accepted. Received.

ABSTRACT

We present ground-based broad-band photometry of two transits in the WASP-44 planetary system obtained simultaneously through four optical (Sloan g' , r' , i' , z') and three near-infrared (NIR ; J , H , K) filters. We achieved low scatters of 1–2 mmag per observation in the optical bands with a cadence of ≈ 48 s, but the NIR -band light curves present much greater scatter. We also observed another transit of WASP-44 b by using a Gunn- r filter and telescope defocussing, with a scatter of 0.37 mmag per point and an observing cadence around 135 s. We used these data to improve measurements of the time of mid-transit and the physical properties of the system. In particular, we improved the radius measurements of the star and planet by factors of 3 and 4, respectively. We find that the radius of WASP-44 b is $1.002 \pm 0.033 \pm 0.018 R_{J_{up}}$ (statistical and systematic errors, respectively), which is slightly smaller than previously thought and differs from that expected for a core-free planet. In addition, with the help of a synthetic spectrum, we investigated the theoretically-predicted variation of the planetary radius as a function of wavelength, covering the range 370–2440 nm. We can rule out extreme variations at optical wavelengths, but unfortunately our data are not precise enough (especially in the NIR bands) to differentiate between the theoretical spectrum and a radius which does not change with wavelength.

Key words: stars: planetary systems – stars: fundamental parameters – stars: individual: WASP-44

1 INTRODUCTION

The *transit method* is not only an excellent technique to detect extrasolar planets, but also provide unrivalled access to their physical parameters. The geometry of a transiting extrasolar planet (TEP) system permits measurement of the mass, radius and density of a planet. These quantities require some input from stellar evolutionary theory, but the planetary surface gravity can be measured directly. A TEP system is therefore a potential *horn of plenty* of physical information on planetary systems (Seager & Sasselov 2000; Sudarsky et al. 2000; Brown et al. 2001; Hubbard et al. 2001; Seager & Mallén-Ornelas 2003; Sudarsky et al. 2003; Charbonneau et al. 2005; Holman & Murray 2005; Winn et al. 2005; Southworth et al. 2007).

Currently, most of the TEPs discovered by ground-based transit surveys (e.g. Hellier et al. 2012; Smalley et al.

2012; Bakos et al. 2012; Hartman et al. 2012; Penev et al. 2013; Bryan et al. 2012; Beatty et al. 2012; Siverd et al. 2012) are close-in hot Jupiters, because the detection probability for such planets is much greater than for those which are smaller or on wider orbits. Hot Jupiters are also relatively straightforward to detect via the *radial velocity method*, as they induce comparatively large velocity variations in their host stars. The existence of hot Jupiters was unexpected (Mayor and Queloz 1995), and led to the birth of new formation and migration theories (see the reviews of D’Angelo et al. 2010 and Lubow and Ida 2010). The bias of the ground-based surveys in favour of this class of planets is clear, whereas the *Kepler* satellite has already found hundreds of smaller and longer-period planet candidates from only 16 months of data (Borucki et al. 2011a,b; Batalha et al. 2012).

Another fascinating opportunity offered by TEPs is the possibility to probe their atmospheres. Due to atomic and molecular absorption, the analysis of the spectrum of the

* mancini@mpia-hd.mpg.de

parent stars during transit (primary eclipse) is an excellent way to probe their atmospheric composition. The existence of two different classes of hot Jupiters (pM and pL) has been suggested according to the incident stellar flux received from the parent star and to the expected amount of absorbing substances, such as gaseous titanium oxide (TiO) and vanadium oxide (VO), in their atmospheres (Fortney et al. 2008). According to theoretical models, these two oxidized elements should be extremely strong absorbers for the pM class between 450 nm and 700 nm, causing such planets to have a hot (~ 2000 K) stratosphere. An observable variation of radius with wavelength, due to the opacities of these elements, is consequently expected in the optical bands (Burrows et al. 2007). The radius of a pM planet should be 3% lower at 350–400 nm versus 500–700 nm. The radius variations for the colder pL-class planets (incident flux $< 10^9$ erg s $^{-1}$ cm $^{-2}$) are smaller, but a significant contribution to the opacity in the optical band is expected from NaI at ~ 590 nm, and KI at ~ 770 nm (Fortney et al. 2008, 2010; Burrows et al. 2010). Transmission spectroscopy is essential for detecting atmospheric absorbers, and is complementary to observations at secondary eclipse which can help to determine the day-side atmospheric temperature structure.

Accurate measurements of planet radii provide critical constraints for astrophysicists working on planet formation and evolution, because they provide an indication of the planet internal heat, structure and composition, as well as the heating mechanism for those which undergo strong tidal effects and stellar irradiation, allowing the discrimination between competing theories (Pollack et al. 1996; Boss 1997). In particular, the most irradiated hot Jupiters are characterised by anomalously inflated radii for which the explanation remains unclear (Bodenheimer et al. 2003; Gu et al. 2004; Gaudi 2005; Fortney et al. 2007; Jackson et al. 2008; Dobbs-Dixon & Lin 2008; Batygin et al. 2009; Ibgui & Burrows 2009; Miller et al. 2009; Ibgui et al. 2010; Laughlin et al. 2011; Miller & Fortney 2011; Demory & Seager 2011).

Photometric and spectroscopic analyses of planet atmospheres started with the use of optical, near-infrared (NIR) and infrared (IR) instruments aboard the *Hubble* and *Spitzer* space telescopes (Charbonneau et al. 2002; Vidal-Madjar et al. 2003, 2004; Richardson et al. 2006; Tinetti et al. 2007; Knutson et al. 2007a,b; Richardson et al. 2007; Swain et al. 2008; Pont et al. 2008; Beaulieu et al. 2008, 2010, 2011; Gillon et al. 2012) and led to the detection of Rayleigh scattering in a few hot Jupiter atmospheres, plus absorption lines associated with H₂O, Na, CH₄, TiO and VO (see above references but also Ballester et al. 2007; Barman 2007; Sing et al. 2008a,b; Lecavelier des Etangs et al. 2008; Désert et al. 2008; Zahnle et al. 2009; Spiegel et al. 2009; Fossati et al. 2010; Tinetti et al. 2010; Désert et al. 2011; Wood et al. 2011; Gibson et al. 2011; Crossfield et al. 2012; Crouzet et al. 2012).

After a number of pioneering experiments with null results, ground-based spectroscopy also obtained some interesting results. Observations performed at the Hobby-Eberly and Subaru telescopes, in the spectral range 500–900 nm, detected Na absorption in the transmission spectrum of HD 189733 b (Redfield et al. 2008) and HD 209458 b (Snellen et al. 2008). NIR spectroscopy of HD 209458 b at the VLT in the range 2291–2349 nm reported a significant

wavelength shift in absorption lines from carbon monoxide in the planet's atmosphere (Snellen et al. 2010).

High-resolution NIR spectroscopic measurements at the Keck telescopes over the wavelength range 2100–2400 nm, revealed an upper limit for CO absorption in the atmosphere of HD 209458 b (Deming et al. 2005), and that the super-Earth GJ 1214 b is a H-dominated planet (Crossfield et al. 2011). GJ 1214 b was also studied through multi-object spectroscopy from 0.61 to 0.85 μ m, and in the *J*, *H*, and *K* atmospheric windows by using VLT/FORS and Magellan/MMIRS, the data being consistent with a featureless transmission spectrum for the planet (Bean et al. 2011).

A radius variation with wavelength was investigated for HD 209458 b by Knutson et al. (2007a) using ten-colour HST photometry. Different analyses of these data have given conflicting results (Knutson et al. 2007a; Barman 2007; Sing et al. 2008a; Southworth 2008). An HST transmission spectrum of HD 189733 b covering 270–570 nm showed a gradual increase of radius towards shorter wavelengths which was interpreted as a result of Rayleigh scattering from a high-altitude atmospheric haze (Sing et al. 2011a). But observations covering 550–1050 nm did not provide any indication of the expected NaI or KI features (Pont et al. 2008), and those in the ranges 1082–1168 nm and 1514–1693 nm did not detect any variation in planetary radius (Gibson et al. 2012a).

Using the Gran Telescopio Canarias (GTC), Sing et al. (2011b) claimed the first evidence for potassium in an extra-solar planet, from photometry of the XO-2 system in four narrow red-optical passbands, by detecting KI absorption at 766.5 nm. This technique was also used by Colón et al. (2012) to study HD 80606 b, who found an unexplained large ($\approx 4.2\%$) change in the apparent planetary radius between the wavelengths 769.9 and 777.4 nm. The differential spectrophotometry technique was used to obtain two transit light curves of XO-2 b with GTC by Sing et al. (2012), who detected significant absorption in the planetary atmosphere in a 50-Å bandpass centred on the NaI doublet. Instead, the presence of an Na-rich atmosphere in WASP-29 b was recently ruled out by Gibson et al. (2012b), using Gemini-South GMOS transit spectrophotometry.

Southworth et al. (2012b) recently presented a study of possible radius variations of the hot Jupiter HAT-P-5 b, based on photometry obtained simultaneous in the *u*, *g*, *r* and *I* passbands. The authors detected a gradual increase of the radius between 450 nm and 850 nm, plus a substantially larger planetary radius at 350 nm. The latter phenomenon can be explained by systematic errors in the *u*-band photometry, but is also consistent with Rayleigh scattering as in the case of HD 189733 b. A similar multi-band investigation of HAT-P-8 (Mancini et al. 2013) suggests the presence of strong optical absorbers near the terminator of this TEP.

Here we focus our attention on the planetary system WASP-44, discovered by Anderson et al. (2012). The system consists of a $0.89 M_{\text{Jup}}$ planet on a 2.42-day orbit around an inactive G8 V star ($V = 12.9$, $[\text{Fe}/\text{H}] = +0.06$). In this work we present the first photometric follow-up since its discovery was announced, covering seven optical/NIR passbands. We refine the physical properties of the system and attempt to probe for radius variations in these passbands.

Our paper is structured as follows. In § 2 we describe the instruments used for the observations and give some

details concerning the data reduction. In § 3 we illustrate the analysis of the data which led to the refinement of the orbital period and the physical properties of the WASP-44 system. Then, we examine the variation of the planetary radius with wavelength. Finally, in § 4 we summarise our results.

2 OBSERVATIONS AND DATA REDUCTION

Two transits of WASP-44 b were recorded on 2011 October 2 and 6, using the Gamma Ray Burst Optical and Near-Infrared Detector (GROND) instrument mounted on the MPG¹/ESO 2.2 m telescope at ESO La Silla, Chile. GROND is an imaging system capable of simultaneous photometric observations in four optical (identical to Sloan g' , r' , i' , z') and three NIR (J , H , K) passbands (Greiner et al. 2008). Each of the four optical channels is equipped with a back-illuminated 2048×2048 E2V CCD, with a field of view (FOV) of $5.4' \times 5.4'$ at a scale of $0.158''/\text{pixel}$. The three NIR channels use 1024×1024 Rockwell HAWAII-1 arrays with a FOV of $10' \times 10'$ at $0.6''/\text{pixel}$.

We applied a slight telescope defocus and obtained repeated integrations during both runs. Autoguiding was used to keep the stars on the same pixels. All images were digitised using the fast read-out mode (~ 10 s) to improve the time sampling. On 2011/10/02 we monitored the flux of WASP-44 in nearly photometric conditions, and saw a monotonically seeing decline from $0.50''$ to $1.03''$ as airmass decreased from 1.08 to 1.05 and then rose to 1.54. Exposures of 20 s were used in the optical channels and stacks of four 4 s images were obtained in the NIR channels. On 2011/10/06 we experienced worse atmospheric conditions, and the airmass changed from 2.07 to 1.05 during our observations. Images with exposure times of 25 s were obtained in the optical channels, and stacks of six 4 s images in the NIR channels. For the optical frames we selected a fast read-out mode, which provided a 15 s readout. Due to the necessary synchronization of the optical and NIR starting times for each exposure, the observing cadence resulted to be of ≈ 48 and ≈ 25 s in the optical and NIR bands respectively.

Another full transit of WASP-44 b was observed through a Gunn r filter on the night of 2011/09/02 using the Wide Field Camera (WFC) on the 2.5 m Isaac Newton Telescope (INT) at La Palma. WFC is an optical mosaic camera consisting of four thinned EEV $2k \times 4k$ CCDs, with a plate scale of $0.33''/\text{pixel}^{-1}$. The telescope was heavily defocussed so the point spread function (PSF) of the target and comparison stars had not more than 35 000 counts per pixel. We used the fast readout mode to reduce readout time down to about 15 s. An exposure time of 2 min per frame was used, and the resulting observing cadence was roughly 135 s. The night was photometric. We were not able to autoguide the telescope as the autoguider is incorporated into the WFC and so was also defocussed. A summary of the observational data is reported in Table 1.

Reduction of the optical frames was undertaken using standard methods. We created master bias and flat-field images by median-combining sets of bias images and sky

Table 2. Excerpts of the light curves of WASP-44. The full dataset will be made available at the CDS.

Telescope	Filter	BJD (TDB)	Diff. mag.	Error
INT	Gunn r	2455807.576418	0.00036	0.00041
INT	Gunn r	2455807.579370	0.00009	0.00042
ESO 2.2m	Sloan g'	2455836.647443	0.00126	0.00100
ESO 2.2m	Sloan g'	2455836.649992	0.00210	0.00123
ESO 2.2m	Sloan r'	2455836.647443	-0.00097	0.00088
ESO 2.2m	Sloan r'	2455836.649992	0.00079	0.00109
ESO 2.2m	Sloan i'	2455836.647443	0.00096	0.00109
ESO 2.2m	Sloan i'	2455836.649992	0.00138	0.00134
ESO 2.2m	Sloan z'	2455836.647443	-0.00143	0.00142
ESO 2.2m	Sloan z'	2455836.649992	0.00100	0.00179

flats, and used them to correct the science images. Aperture photometry was performed using the IDL²/ASTROLIB³ implementation of DAOPHOT (Stetson 1987; Southworth et al. 2009). The apertures were placed manually and shifted to account for pointing variations, which were measured by cross-correlating each image against a reference image. We experimented with wide range of aperture sizes and retained those which gave photometry with the lowest scatter compared to a fitted model. The times of observation were converted from UTC to BJD(TDB) using the IDL procedures of Eastman et al. (2010).

Differential photometry was obtained in each filter using between two and four comparison stars, two of which were enough bright to produce count rates comparable to those of WASP-44. All good comparison stars were combined into one ensemble by weighted flux summation. Slow variations in the apparent brightness of the reference stars, primarily attributable to atmospheric effects, were treated by fitting a polynomial to regions outside transit, whilst simultaneously optimising the weights of the comparison stars. Given the limited number of comparison stars in the small field of view of GROND, and the shape of the slow brightness variations, we used a second-order polynomial versus time. Uncertainties introduced by this procedure were considered in the modelling of the light curves, as described in the next section.

The NIR frames were also calibrated in a standard way, including dark subtraction, flat correction and sky subtraction. The master sky images used in sky subtraction were created from two sets of 20-position dithering sky measurements, one before the science observation and one after. We performed aperture photometry on the calibrated NIR images as well. The aperture locations were determined using IDL/FIND. Various combinations of aperture and annulus sizes were checked to find the best photometry. We also carefully made ensembles of comparison stars, and chose the group which showed the least deviation from the target. After normalising the target light curve with the composite reference light curve, we decorrelated the data with position, seeing and airmass in order to remove the correlated

¹ Max Planck Gesellschaft.

² The acronym IDL stands for Interactive Data Language and is a trademark of ITT Visual Information Solutions. For further details see <http://www.ittvis.com/ProductsServices/IDL.aspx>.

³ <http://idlastro.gsfc.nasa.gov/>

Table 1. Log of the observations presented in this work. N_{obs} is the number of observations and “Moon illum.” is the fractional illumination of the Moon at the midpoint of the transit. The aperture sizes are the radii of the software apertures for the star, inner sky and outer sky, respectively. β is the factor used to inflate the errorbars (see § 3). Transit #1 was observed using the 2.5 m INT in La Palma, whereas transits #2 and #3 using the MPG/ESO 2.2 m telescope in La Silla.

Transit	Date	Start/end Time (UT)	N_{obs}	Exposure time (s)	Filter	Airmass	Moon illum.	Aperture sizes (px)	Scatter (mmag)	β
1	2011 09 03	00:28 - 00:57	156	120	Gunn r	1.60 → 1.32 → 2.18	31%	25, 35, 50	0.37	1.15
2	2011 10 02	03:21 - 07:35	317	20	Sloan g'	1.08 → 1.05 → 1.54	40%	16, 35, 55	1.23	1.07
2	2011 10 02	03:21 - 07:35	317	20	Sloan r'	1.08 → 1.05 → 1.54	40%	17, 40, 60	1.08	1.00
2	2011 10 02	03:21 - 07:35	317	20	Sloan i'	1.08 → 1.05 → 1.54	40%	20, 30, 45	1.34	1.00
2	2011 10 02	03:21 - 07:35	317	20	Sloan z'	1.08 → 1.05 → 1.54	40%	12, 25, 40	1.79	1.10
2	2011 10 02	03:21 - 07:35	631	3	J	1.08 → 1.05 → 1.54	40%	6.0, 15.0, 23.0	7.66	1.09
2	2011 10 02	03:21 - 07:35	631	3	H	1.08 → 1.05 → 1.54	40%	2.5, 11.5, 21.0	8.11	1.08
2	2011 10 02	03:21 - 07:35	631	3	K	1.08 → 1.05 → 1.54	40%	3.0, 11.0, 21.0	5.98	1.15
3	2011 10 06	03:21 - 07:35	317	25	Sloan g'	2.07 → 1.05	80%	19, 30, 50	1.89	1.06
3	2011 10 06	03:21 - 07:35	313	25	Sloan r'	2.07 → 1.05	80%	22, 40, 60	1.70	1.32
3	2011 10 06	03:21 - 07:35	313	25	Sloan i'	2.07 → 1.05	80%	20, 40, 60	1.79	1.35
3	2011 10 06	03:21 - 07:35	313	25	Sloan z'	2.07 → 1.05	80%	16, 40, 60	2.52	1.26
3	2011 10 06	03:21 - 07:35	623	3	J	2.07 → 1.05	80%	9.0, 17.0, 25.0	5.23	1.38
3	2011 10 06	03:21 - 07:35	623	3	H	2.07 → 1.05	80%	6.5, 13.5, 22.0	6.96	1.34
3	2011 10 06	03:21 - 07:35	623	3	K	2.07 → 1.05	80%	3.5, 4.5, 18.0	7.65	1.04

red noise. We extracted the optimal NIR light curves for the two nights according to the *rms* of O–C residuals and consistency of the transit depth between two nights. Details are given in Appendix A. The resulting photometry is given in Table 2.

Although we have performed all the possible calibrations and corrections, the scatter of the NIR data is much larger than that of the optical data, and the NIR light curves are heavily dominated by red noise. This problem is related to the adopted observing strategy that unfortunately did not allow a good SNR to be obtained⁴.

Our analysis also included the dataset presented by Anderson et al. (2012), which was obtained through a Gunn r filter and using EulerCam mounted on the 1.2 m Euler-Swiss telescope at ESO La Silla.

3 ANALYSIS

We have measured the physical properties of the WASP-44 planetary system following the methodology of the *Homogeneous Studies* project (Southworth 2008, 2009, 2010, 2011, 2012). We refer the reader to those works for a detailed description of the approach.

Since the absolute values of the observational errors from our pipeline (which come ultimately from the APER subroutine) were found to be underestimated, we adopt the standard practice of rescaling them for each dataset to give a reduced χ^2 of $\chi^2_\nu = 1$. Then, in order to account for time-correlated errors (i.e. red noise, which can significantly affect ground-based data) and derive more realistic uncertainties, we inflated the errorbars further by multiplying the data

⁴ After these first observations, we changed our observing strategy adopting the *defocussing* technique for GROND. Thanks to this approach, we can now obtain scatter smaller than 2 mmag per observation in the NIR bands and smaller than 1 mmag in the optical ones, without compromising the sampling (Nikolov et al., in prep.).

weights by a factor $\beta \geq 1$. The β approach (e.g. Pont et al. 2006; Winn et al. 2007) is a widely used way to assess red noise (e.g. Gillon et al. 2006; Winn et al. 2008, 2009; Gibson et al. 2008; Nikolov et al. 2012; Southworth et al. 2012a,b). The factor β is a measurement of how close the data noise is to the Poisson approximation, and is found by binning the data and evaluating the ratio between the size of the residuals versus what would be expected if the data followed Poisson statistics. We evaluated values of the β factor for each individual transit and for groups of 10 datapoints; they are reported in Table 1. For a more exhaustive discussion about rescaling errorbars, see Andrae (2010).

3.1 Period determination

As a first step, we fitted each light curve individually using the JKTEBOP code (see § 3.2) in order to find the transit times. Their uncertainties were estimated from Monte Carlo simulations. To these we added two timings obtained by Anderson et al. (2012) and four obtained by amateur astronomers, which are available on the TRESCA⁵ website (see Table 3). We excluded from this analysis our NIR data since they are much noisier than the optical ones. All timings were placed on BJD(TDB) time system. The resulting measurements of transit midpoints were fitted with a straight line to obtain a new orbital ephemeris:

$$T_0 = \text{BJD(TDB)} 2455434.37642(37) + 2.4238133(23) \times E \quad (1)$$

where E is the number of orbital cycles after the reference epoch (the midpoint of the first transit observed by Anderson et al. 2012) and quantities in brackets denote the uncertainty in the final digit of the preceding number. The fit has $\chi^2_\nu = 2.42$, so the uncertainties were increased to account for this. Despite this large χ^2_ν , we do not note any

⁵ The TRansiting ExoplanetS and CAndidates (TRESCA) website can be found at <http://var2.astro.cz/EN/tresca/index.php>

Table 3. Central transit times of WASP-44 and their residuals versus the ephemeris derived in this work. TRESCA refers to the “Transiting ExoplanetS and CAndidates” website.

Central transit time BJD(TDB) – 2400000	Cycle no.	Residual (JD)	Reference
55434.37637 ± 0.00040	0	-0.00005	Anderson et al. (2012)
55453.76639 ± 0.00042	8	-0.00054	Anderson et al. (2012)
55807.64374 ± 0.00013	154	0.00007	This work (INT r)
55814.91655 ± 0.00150	157	0.00144	Evans P. (TRESCA)
55829.45489 ± 0.00245	163	-0.00310	Lomoz F. (TRESCA)
55829.46151 ± 0.00163	163	0.00315	Lomoz F. (TRESCA)
55836.72905 ± 0.00020	166	-0.00038	This work (GROND g')
55836.72979 ± 0.00030	166	0.00036	This work (GROND r')
55836.72900 ± 0.00020	166	-0.00043	This work (GROND i')
55836.72928 ± 0.00015	166	-0.00015	This work (GROND z')
55841.57719 ± 0.00035	168	0.00014	This work (GROND g')
55841.57757 ± 0.00046	168	0.00052	This work (GROND r')
55841.57684 ± 0.00028	168	-0.00021	This work (GROND i')
55841.57769 ± 0.00031	168	0.00064	This work (GROND z')
56127.58624 ± 0.00048	286	-0.00078	Sauer T. (TRESCA)

systematic deviation from the predicted transit times. A plot of the residuals around the fit is shown in Fig. 1. Since the number of known observed transits of this planet is still very low, no conclusions can be drawn regarding the existence of any third body in the system.

3.2 Light curve modelling

The light curves were modelled using the JKTEBOP⁶ code. The primary fitted parameters were the sum and ratio of the fractional radii of the star and planet, $r_A + r_b$ and $k = r_b/r_A$, and the orbital inclination, i . The fractional radii of the components are defined as $r_A = R_A/a$ and $r_b = R_b/a$, where a is the orbital semimajor axis, and R_A and R_b are the true radii of the two objects. Additional parameters of the fit included the light level outside transit and the midpoint of the transit. Limb darkening (LD) was imposed using a quadratic law and the corresponding coefficients fixed at values theoretically predicted using model atmospheres (Claret 2004). Southworth (2008) performed three different treatments of the LD coefficients: (i) both coefficients fixed to theoretical values; (ii) both coefficients fitted; (iii) the linear LD coefficient fitted and the nonlinear one fixed to its theoretically predicted value. While the second treatment is possible only when the data are of high quality, the use of the third alternative has a negligible impact on the final results. Uncertainties were calculated using both Monte Carlo simulations and a residual-permutation algorithm (Southworth 2008), and the larger of the two values was retained for each output quantity. The orbital eccentricity was fixed to zero (Anderson et al. 2012). All the datasets were solved individually. As in the previous section, due to their large scatter (see Table 1), we did not use the NIR data for estimating the physical properties of the planetary system.

Representative photometric parameters were obtained for each dataset and are given in Table 4. The corresponding

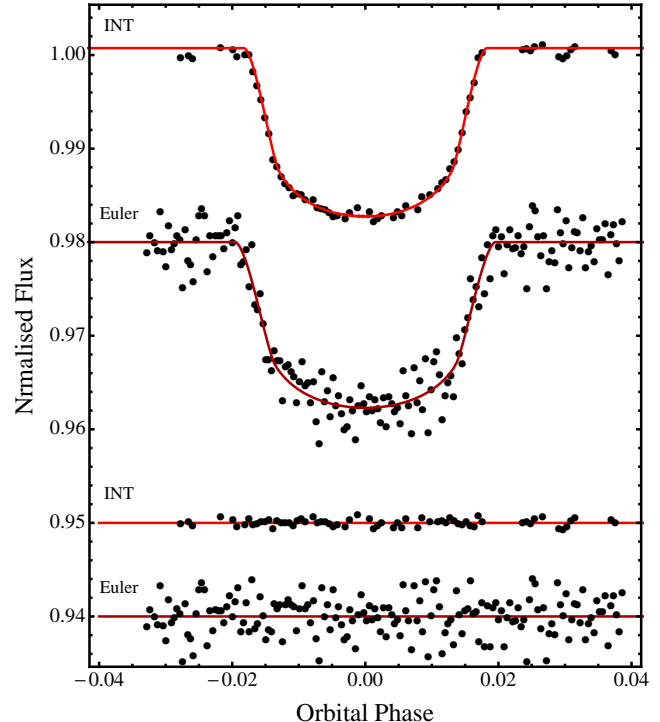


Figure 4. As for Fig. 2 but for the r -filter INT and Euler (Anderson et al. 2012) light curves of WASP-44.

best fits are shown in Fig. 2 and 3 for the GROND data and in Fig. 4 for the INT and Euler data. The final photometric parameters are the weighted mean of the values for each dataset. The agreement between light curves is excellent: the χ^2_ν value of the agreement of the individual parameters with respect to the weighted mean is smaller than 0.75 for all except k , where we found a modestly larger χ^2_ν of 1.64. We have found this situation to be common during our work on the *Homogeneous Studies* papers. Table 4 also shows a comparison with the results from Anderson et al. (2012), which are in good agreement with ours but have much larger errorbars.

3.3 Physical properties of the WASP-44 system

Following the approach described in Southworth (2009), the estimation of the physical properties of the WASP-44 system was performed making use of standard formula (e.g. Hilditch 2001). We used the photometric parameters measured in § 3.2, and the velocity amplitude, effective temperature, and metallicity of the star ($K_A = 138.8 \pm 9.0 \text{ km s}^{-1}$, $T_{\text{eff}} = 5410 \pm 150 \text{ K}$, $[\text{Fe}/\text{H}] = +0.06 \pm 10$) measured by Anderson et al. (2012). We interpolated within tabulations from theoretical stellar models to find the best agreement between the observed and model-predicted T_{eff} , and the measured r_A and calculated R_A/a . This yielded the best-fitting mass, radius, surface gravity and mean density of the star (M_A , R_A , $\log g_A$ and ρ_A) and of the planet (M_b , R_b , g_b and ρ_b). We also calculated the orbital semi-major axis (a), planetary equilibrium temperature (T_{eq}), Safranov number (Θ), and the evolutionary age of the star.

The uncertainties in the input parameters were propagated into the output physical properties using a pertur-

⁶ JKTEBOP is written in FORTRAN77 and the source code is available at <http://www.astro.keele.ac.uk/~jkt/>

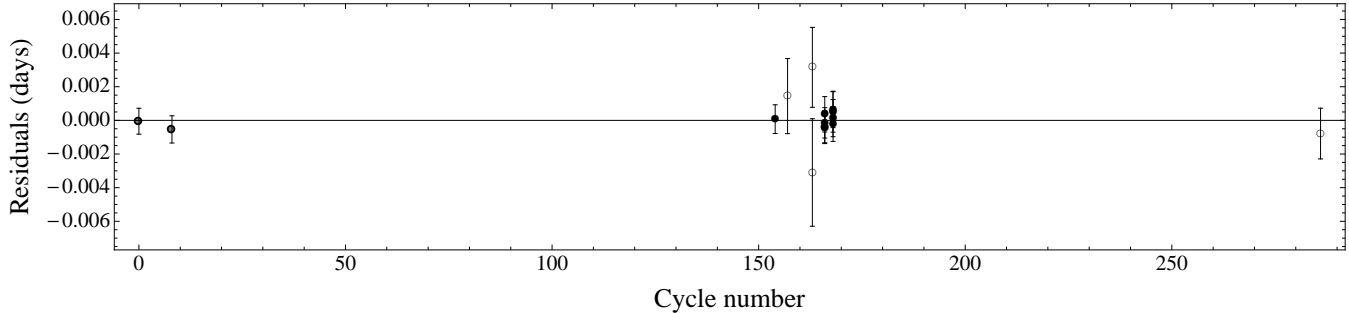


Figure 1. O-C diagram of the mid-transit times of WASP-44 b versus a linear ephemeris. The timings in black are from this work, and in grey are from Anderson et al. (2012). The timings obtained by amateur astronomers are plotted using open circles. The uncertainties of our points have been rescaled (see text).

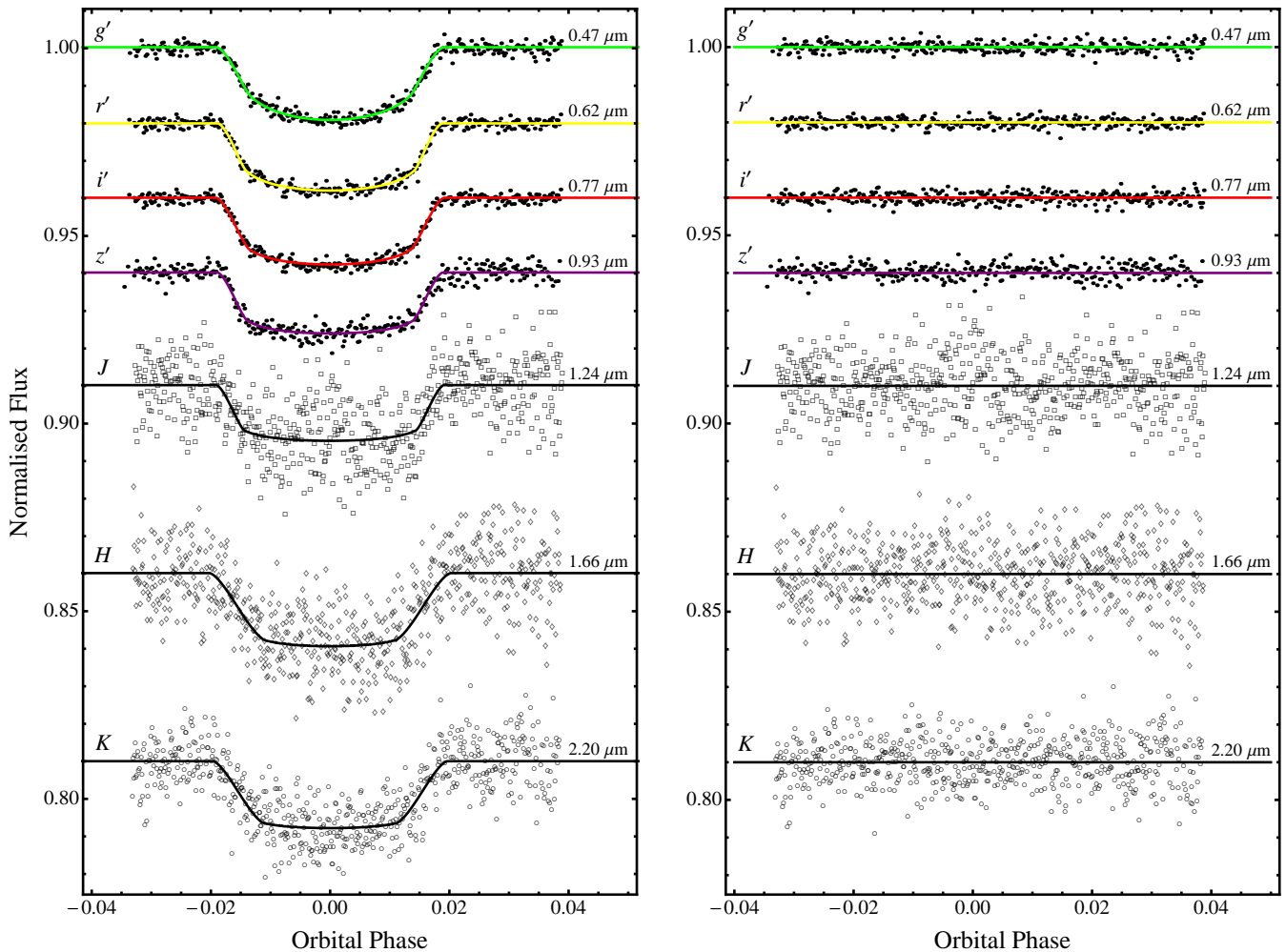


Figure 2. First set (2011/10/02) of GROND light curves of WASP-44 compared to the best JKTEBOP fits using the quadratic LD law. The residuals of the fits are plotted at the base of the figure, offset from zero.

bation analysis (Southworth et al. 2005). Systematic errors were assessed by comparing results from five different sets of theoretical models (see Southworth 2010). The sets of physical properties found using each set of stellar models is shown in Table 5 and the final physical properties of the WASP-44 system are given in Table 6. The results obtained by Anderson et al. (2012) are less precise but are in good

agreement with our own. In particular, we improved the measurement precisions of the radii of both the planet and the parent star, by factors of 4 and 3 respectively. The radius of WASP-44 b that we found ($1.002 \pm 0.033 \pm 0.018 R_{Jup}$) is smaller than that measured in the discovery paper and does not match the predicted radii of coreless hot-Jupiter planets as estimated by Fortney et al. (2007). According to their

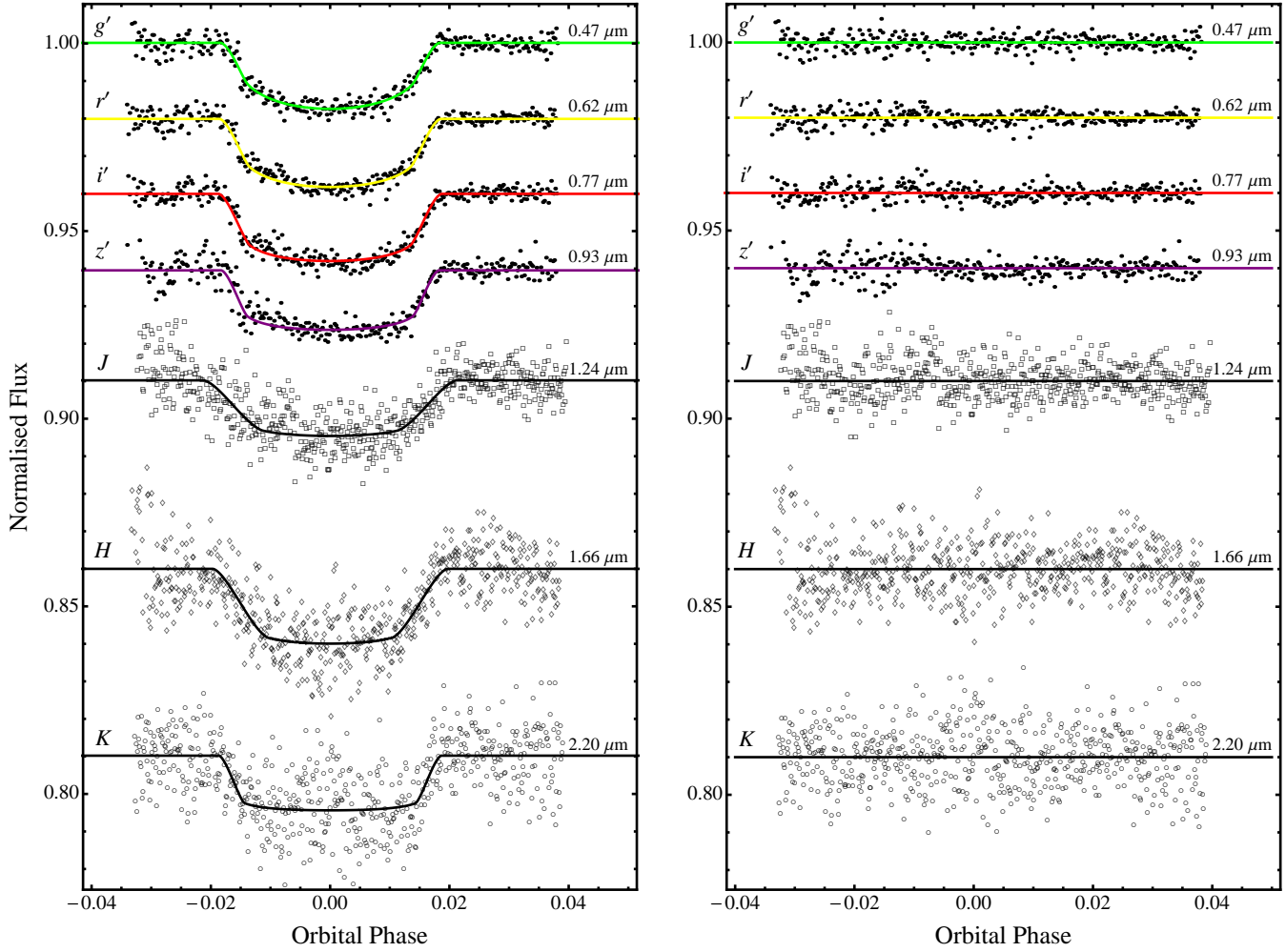


Figure 3. Second set (2011/10/06) of GROND light curves of WASP-44 compared to the best JKTEBOP fits using the quadratic LD law. The residuals of the fits are plotted at the base of the figure, offset from zero.

Table 4. Parameters of the fits to the ten light curves of WASP-44. The final parameters are the weighted mean of the result for the GROND, INT and Euler light curves.

Source	$r_A + r_b$	k	i°	r_A	r_b
GROND g' -band #1	0.1368 ± 0.0056	0.1228 ± 0.0023	86.2 ± 0.5	0.1218 ± 0.0020	0.01496 ± 0.00086
GROND g' -band #2	0.139 ± 0.010	0.1188 ± 0.0028	86.2 ± 1.0	0.1240 ± 0.0090	0.0147 ± 0.0014
GROND r' -band #1	0.1268 ± 0.0045	0.1175 ± 0.0014	87.3 ± 0.6	0.1135 ± 0.0039	0.01333 ± 0.00060
GROND r' -band #2	0.1284 ± 0.0080	0.1190 ± 0.0029	86.9 ± 0.8	0.1147 ± 0.0068	0.0136 ± 0.0011
GROND i' -band #1	0.1363 ± 0.0051	0.1205 ± 0.0016	86.3 ± 0.5	0.1216 ± 0.0044	0.0147 ± 0.00068
GROND i' -band #2	0.1303 ± 0.0087	0.1204 ± 0.0029	86.7 ± 0.9	0.1163 ± 0.0076	0.0140 ± 0.0011
GROND z' -band #1	0.1306 ± 0.0075	0.1153 ± 0.0023	86.8 ± 0.8	0.1171 ± 0.0065	0.01349 ± 0.00095
GROND z' -band #2	0.123 ± 0.010	0.1134 ± 0.0034	87.4 ± 1.5	0.1102 ± 0.0089	0.0125 ± 0.0013
INT r -band	0.1285 ± 0.0029	0.1196 ± 0.0013	86.6 ± 0.3	0.1148 ± 0.0026	0.01373 ± 0.00042
Euler r -band	0.141 ± 0.011	0.1197 ± 0.0039	85.9 ± 1.0	0.1261 ± 0.0100	0.0151 ± 0.0016
Final results			86.59 ± 0.18	0.1168 ± 0.0016	0.0139 ± 0.0002
Anderson et al. (2012)	0.1398	0.1260 ± 0.0030	$86.02^{+1.11}_{-0.86}$	0.1242 ± 0.0102	0.0157

Table 5. Derived physical properties of WASP-44 from using each of five different theoretical stellar models. In each case $g_b = 21.5 \pm 1.6 \text{ m s}^{-2}$, $\rho_A = 1.414 \pm 0.058 \rho_\odot$ and $T_{\text{eq}} = 1304 \pm 37 \text{ K}$.

	This work (Claret models)	This work (Y ² models)	This work (Teramo models)	This work (VRSS models)	This work (DSEP models)
K_b (km s ⁻¹)	156.1 ± 4.1	151.7 ± 1.0	152.6 ± 4.2	152.7 ± 4.1	153.7 ± 3.2
M_A (M_\odot)	0.968 ± 0.077	0.888 ± 0.018	0.904 ± 0.074	0.907 ± 0.073	0.924 ± 0.058
R_A (R_\odot)	0.881 ± 0.025	0.856 ± 0.016	0.862 ± 0.024	0.862 ± 0.024	0.865 ± 0.020
$\log g_A$ (cgs)	4.534 ± 0.018	4.521 ± 0.010	4.524 ± 0.018	4.524 ± 0.018	4.530 ± 0.016
M_b (M_{Jup})	0.901 ± 0.075	0.851 ± 0.056	0.861 ± 0.073	0.863 ± 0.073	0.874 ± 0.067
R_b (R_{Jup})	1.020 ± 0.033	0.992 ± 0.019	0.997 ± 0.033	0.998 ± 0.032	0.994 ± 0.027
ρ_b (ρ_{Jup})	0.793 ± 0.070	0.816 ± 0.069	0.812 ± 0.072	0.811 ± 0.072	0.831 ± 0.071
Θ	0.0640 ± 0.0046	0.0658 ± 0.0045	0.0654 ± 0.0048	0.0654 ± 0.0047	0.0656 ± 0.0046
a (AU)	0.03508 ± 0.00093	0.03409 ± 0.00023	0.03429 ± 0.00093	0.03432 ± 0.00092	0.03454 ± 0.00072

Table 6. Final physical properties of the WASP-44 system. The first errorbar for each parameter is the statistical error, which stems from the measured spectroscopic and photometric parameters. The second errorbar is the systematic error arising from the use of theoretical stellar models, and is given only for those parameters which have a dependence on stellar theory. The results from Anderson et al. (2012) are included for comparison.

	This work (final)	Anderson et al. (2012)
M_A (M_\odot)	$0.917 \pm 0.077 \pm 0.051$	0.951 ± 0.034
R_A (R_\odot)	$0.865 \pm 0.025 \pm 0.016$	$0.927^{+0.068}_{-0.074}$
$\log g_A$ (cgs)	$4.526 \pm 0.018 \pm 0.008$	$4.481^{+0.068}_{-0.057}$
ρ_A (ρ_\odot)	1.414 ± 0.058	$1.19^{+0.32}_{-0.22}$
M_b (M_{Jup})	$0.869 \pm 0.075 \pm 0.032$	0.889 ± 0.062
R_b (R_{Jup})	$1.002 \pm 0.033 \pm 0.018$	1.14 ± 0.11
g_b (ms ⁻²)	21.5 ± 1.6	$15.7^{+3.4}_{-3.0}$
ρ_b (ρ_{Jup})	$0.808 \pm 0.072 \pm 0.015$	$0.61^{+0.23}_{-0.15}$
T_{eq} (K)	1304 ± 37	1343 ± 64
Θ	$0.0652 \pm 0.0048 \pm 0.0012$	—
a (AU)	$0.03445 \pm 0.00093 \pm 0.00063$	0.03473 ± 0.00041
Age (Gyr)	$4.1^{+5.9}_{-6.0} {}^{+4.1}_{-2.4}$	—

tables⁷, a $0.875 M_J$ planet with $50 M_{\text{Earth}}$ core at 0.045 AU from the Sun (age 3.16 Gyr), is $0.991 R_{\text{Jup}}$. On the contrary, the expected radius for a core-free planet with the same properties is $1.119 R_{\text{Jup}}$.

3.4 Variation of planetary radius with wavelength

As an additional possibility for the GROND data, we made an attempt to investigate the possible variation of the radius of WASP-44 b with wavelength. This is quite a difficult task because the relative faintness of the host star ($V \sim 12.9$) makes this system less than ideal for optical photometric studies, especially from the ground. Moreover, as already mentioned, our *in-focus* observing strategy has proved to be ill-suited to obtaining high-precision photometry, particularly in the NIR bands. Finally, by using broad-band filters we are forced to average our measurements of the planet radius in each band over a quite larger range of the wavelength (the best case in the i' filter where its width is “only” 100

⁷ The tables, interpolated from the giant planet thermal evolution models described in Fortney et al. (2007), are available at <http://www.ucolick.org/~jfortney/models.htm>

nm). For these reasons, the results of this section should be used with care.

The GROND instrument was conceived only for the follow-up of gamma-ray bursts, and was not designed to allow filter changes for individual observing sequences. We were therefore unable to use filters with narrow passbands covering specific wavelength ranges. We note that the four optical bands of GROND were already used by de Mooij et al. (2012) to investigate the atmosphere of GJ 1214 b, a $6.55 M_\oplus$ transiting planet. Here we try for the first time to use all the seven bands, exploiting the full potential of GROND.

Following the same strategy used by Southworth et al. (2012b) and Mancini et al. (2013), we proceeded as follows. The two GROND datasets were combined by phase and according to passband, and then fitted with all parameters fixed to the final values given in Table 4, with the exception of k . The LD coefficients were fixed to theoretical values. The errors were estimated by a residual-permutation algorithm (Southworth 2008). This approach removes sources of uncertainty common to all datasets, allowing us to maximise the accuracy of estimations of the fractional planetary radius $r_b = R_b/a$ as a function of wavelength and with relative errorbars only. The results are displayed in Fig. 5, where the points show the data, the vertical bars represent the relative errors in the measurements and the horizontal bars indicate the full widths at half maximum transmission of the passbands used. The transmission curves are also reported for completeness. As expected, the uncertainties in the NIR bands are larger, due to the larger scatter and systematic features in the light curves.

Inspection of Fig. 5 shows that our measurements are unfortunately not sufficiently accurate to claim a clear variation of r_b along the seven passbands. Using the planetary system values reported in Table 6, we computed a one-dimensional model atmosphere of WASP-44 b, using the atmosphere code described in Fortney et al. (2005, 2008). The fully non-gray model uses the chemical equilibrium abundances of Lodders & Fegley (2002) and the opacity database described in Freedman et al. (2008). The atmospheric pressure-temperature profile simulates planet-wide average conditions. We furthermore computed the transmission spectrum of the model using the methods described in Fortney et al. (2010).

At optical wavelengths, r_b appears to be slightly larger in r' and i' than g' and z' . This is as expected for a planet

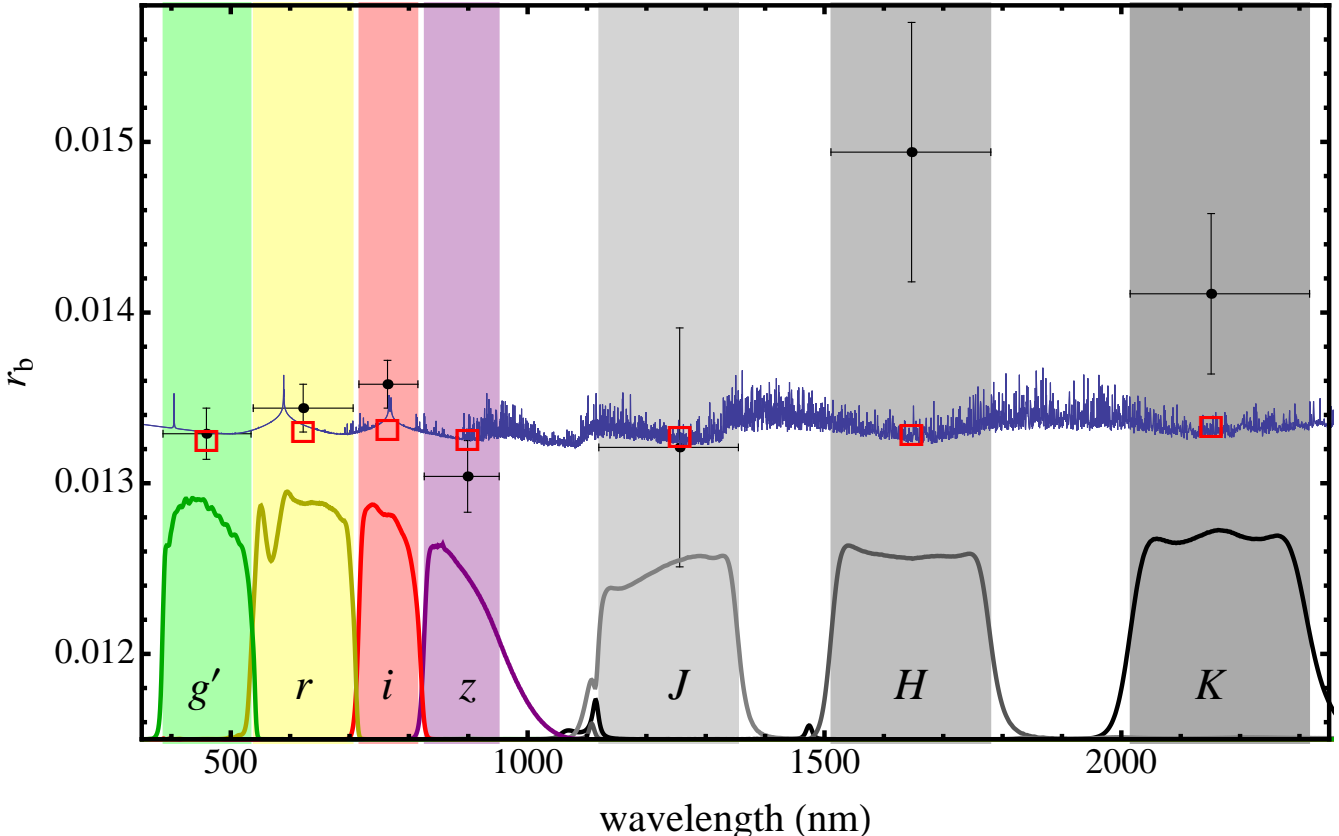


Figure 5. Variation of the fractional planetary radius $r_b = R_b/a$ with wavelength. The points shown in the plot are from the MPG/ESO 2.2 m telescope. The vertical bars represent the errors in the measurements and the horizontal bars show the full widths at half maximum transmission of the passbands used. The solid, blue continuous line is the calculated synthetic spectrum based on a theoretical model of the atmosphere of WASP-44 b. Red boxes indicate the predicted values for this model integrated over the passbands of the observations. Transmission curves of the GROND filters are shown at the bottom of the figure.

with an equilibrium temperature $T_{\text{eq}} \approx 1300$ K, due to the larger predicted radius around the Na and K lines. Although a similar effect is seen in the model (Figure 6), our data are not sufficiently precise to reject the default hypothesis that r_b is constant with wavelength. The radius of WASP-44 b is in agreement with the theoretical model in the J band, but is larger in the H and K bands. We found that the r_b in r' is 9.5% and 4.7% smaller than that for the H and K band respectively, which correspond to a difference in units of atmospheric pressure scale height (H) of roughly $23H$ and $10H$, respectively. The first difference is very large, and would involve an extreme opacity in H .

A more plausible alternative is that the NIR photometry is affected by systematics or correlated noise, which was not possible to eliminate. This is also suggested by the poor SNR observed in the data, which is reflected in the higher scatter of the points in the J , H , K light curves and the different shapes of the fit in the same band between the first and the second observed transits (Figs. 2 and 3). We deduce that systematic errors in the NIR dominate the error budget at these wavelengths.

4 SUMMARY AND DISCUSSION

In this work we have presented the first photometric follow-up of the transiting extrasolar planetary system WASP-44. One transit was observed using WFC on the INT, and two transits were observed in seven passbands simultaneously using GROND on the MPG/ESO 2.2 m telescope. Using these new datasets plus another one taken from the literature (Anderson et al. 2012), we have obtained improved measurements of the orbital ephemerides and physical properties of the system. In particular, we found that the radius of WASP-44 b is smaller than previously found, and is different (at 2σ confidence level) from that theoretically expected for a free-core planet (Fortney et al. 2007). This suggests that WASP-44 b is a “heavy element rich” planet, with the heavy elements being in a distinct core or mixed within the H/He envelope. Such a result is important in order to draw an accurate *mass-radius* plot for TEPs, which provides key diagnostic for theoretical works that look to infer the bulk composition of the giant planets and distinguish them (in some cases) from brown dwarfs.

Although GROND was not designed for follow-up studies of planetary transits, it is one of the very few imaging systems worldwide able to perform simultaneous photometric multi-band observations. The later fact makes GROND an efficient and very useful instrument to detect transit anom-

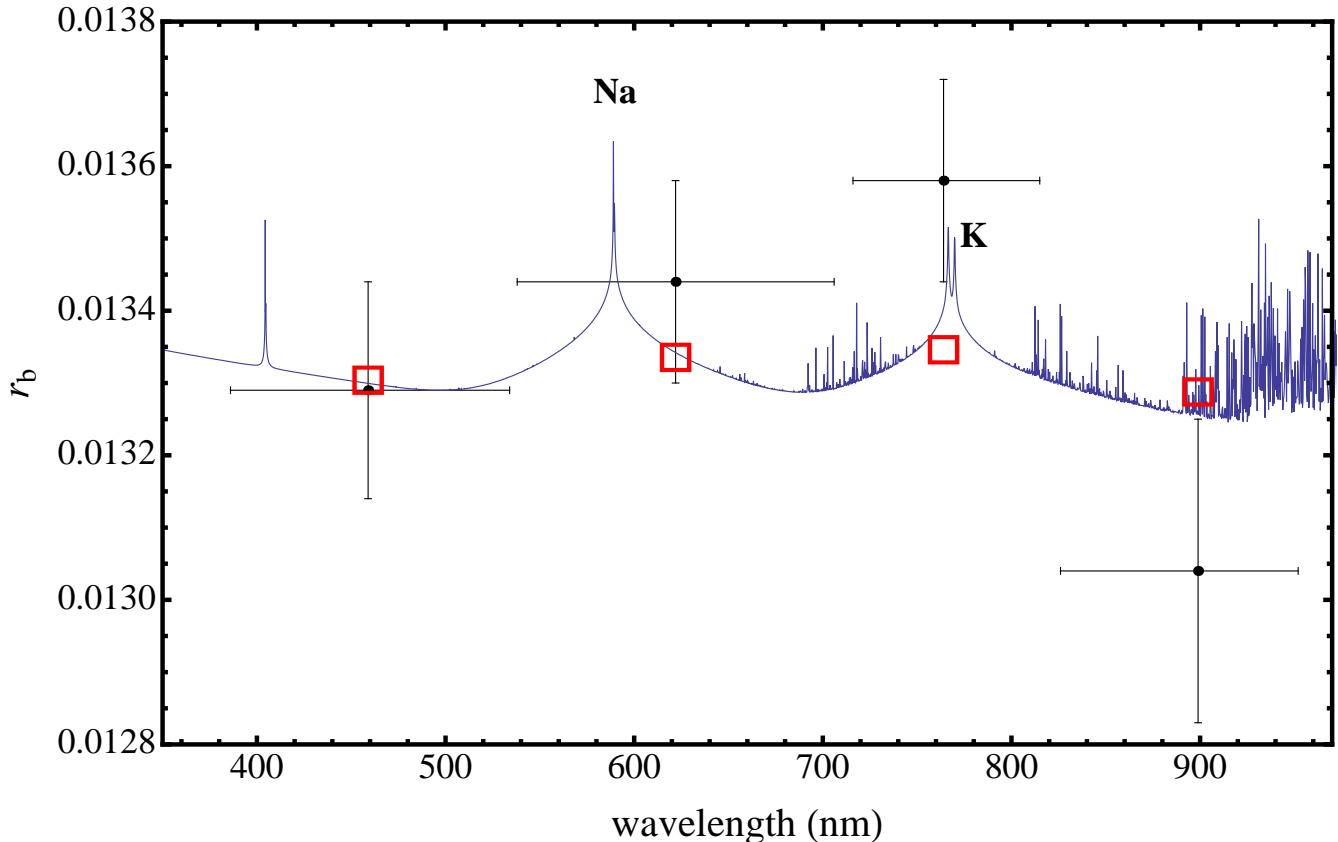


Figure 6. As in Fig. 5 but zoomed in on the optical wavelengths. In this range, the synthetic transmission spectrum is dominated by gaseous Na and K.

lies or to probe the atmosphere of TEPs. Indeed, atomic and molecular absorption as well as scattering processes may result in detectable radius variations as a function of wavelength (Fortney et al. 2007; Batygin et al. 2009). de Mooij et al. (2012) already used GROND in the case of GJ 1214 b, but they restricted their analysis only to the optical bands. Here, for the first time, we used all the seven band of this powerful instrument, to search for variations of the radius of WASP-44 b with wavelength. We measured the planetary radius in the seven GROND passbands, corresponding to a wavelength coverage of 370–2440 nm, and compared them to a synthetic spectrum based on an isothermal model atmosphere in chemical equilibrium. The model reproduces the radius values in the optical, in agreement with the equilibrium temperature of WASP-44 b but, our data lack the precision to rule out the possibility that the planetary radius does not vary with wavelength. It does not predict the radius values found in the *H* and *K* bands, which differ by roughly 23 and 10 atmospheric pressure scale heights to those in the other bands. This phenomenon is most likely due to the comparatively low quality of the NIR data. We have worked to reduce the sources of noise in the subsequent uses of the GROND instrument. More enticing results were obtained for other TEPs and will be shown in forthcoming papers.

ACKNOWLEDGMENTS

Based on observations collected at the MPG/ESO 2.2 m Telescope located at ESO La Silla, Chile. Operations of this telescope are jointly performed by the Max Planck Gesellschaft and the European Southern Observatory. GROND has been built by the high-energy group of MPE in collaboration with the LSW Tautenburg and ESO, and is operating as a PI-instrument at the MPG/ESO 2.2 m telescope. We thank David Anderson for supplying photometric data, and Timo Anguita and Régis Lachaume for their technical assistance during the observations. We thank the anonymous referee for their useful criticisms and suggestions that helped us to improve the quality of the present paper. The reduced light curves presented in this work will be made available at the CDS (<http://cdsweb.u-strasbg.fr/>). JS acknowledges financial support from STFC in the form of an Advanced Fellowship.

REFERENCES

- Anderson, D. R., Collier Cameron, A., Gillon, M., et al. 2012, MNRAS, 422, 1988
- Andrae, R. 2010, arXiv:1009.2755
- Ballester, G. E., Sing, D. K., & Herbert, F. 2007, Nature, 445, 511
- Bakos, G. Á., Hartman, J. D., Torres, G., et al. 2012, AJ, 144, 19

Barman, T. 2007, *ApJ*, 661, L191

Batalha, N. M., Rowe J. F., Bryson S. T., et al. 2012, Submitted to *ApJS*, arXiv:1202.5852

Batygin, K., Bodenheimer, P., Laughlin, G. 2009, *ApJ*, 704, L49

Bean, J. L., Désert, J.-M., Kabath, P., et al. 2011, *ApJ*, 743, 92

Beatty, T. G., Pepper, J. Siverd, R. J., et al. 2012, 2012, *ApJ*, 756, 39

Beaulieu, J. P., Carey, S., Ribas, I., & Tinetti, G. 2008, *ApJ*, 677, 1343

Beaulieu, J. P., Kipping, D. M., Batista, V., et al. 2010, *ApJ*, 409, 963

Beaulieu, J. P., Tinetti, G., Kipping, D. M., et al. 2011, *ApJ*, 731, 16

Bodenheimer, P., Laughlin, G., & Lin, D. N. C. 2003, *ApJ*, 592, 555

Borucki, W. J., Koch, D. G., Basri, G., et al. 2011a, *ApJ*, 728, 117

Borucki, W. J., Koch, D. G., Basri, G., et al. 2011b, *ApJ*, 736, 19

Boss, A. P., 1997, *Science*, 276, 1836

Brown, T. M. 2001, *ApJ*, 553, 1006

Bryan, M. L., Alsubai, K. A., Latham, D. W., et al. 2012, *ApJ*, 750, 84

Burrows, A., Hubeny, I., Budaj, J., & Hubbard, W. B., 2007, *ApJ*, 661, 502

Burrows, A., Rauscher, E., Spiegel, D. S., & Menou, K. 2010, *ApJ*, 719, 341

Charbonneau, D., Brown, T. M., Noyes, R. W., & Gilliland, R. L. 2002, *ApJ*, 568, 377

Charbonneau, D., Allen, L. E., Megeath, S. T., et al. 2005, *ApJ*, 626, 523

Charbonneau, D., Berta, Z. K., Irwin, J., et al. 2009, *Nature*, 462, 891

Claret A., 2004, *A&A*, 428, 1001

Colón, K. D., Ford, E. B., Redfield, S., Fortney, J. J., Shabram, M., Deeg, H. J., & Mahadevan, S. 2012, *MNRAS*, 419, 2233

Crossfield, I. J. M., Barman, T., & Hansen, B. M. S. 2011, *ApJ*, 736, 132

Crossfield, I. J. M., Knutson, H., Fortney, J. J., et al. 2012, *ApJ*, 752, 81

Crouzet, N., McCullough, P. R., Burke, C. J., Long, Douglas 2012, *ApJ*, 761, 7

D'Angelo, G., Durisen, R. H., Lissauer, J. J. 2010, *Exoplanets*, edited by S. Seager. (University of Arizona Press), p. 319

Daemgen, S., Hormuth, F., Brandner, W., Bergfors, C., Janson, M., Hippler, S., & Henning, T. 2009, *A&A*, 498, 567

Deming, D., Brown, T. M., Charbonneau, D., Harrington, J., & Richardson, L. J. 2005, *ApJ*, 622, 1149

de Mooij, E. J. W., Brogi, M., de Kok, R. J., et al. 2012, *A&A*, 538, A46

Demory, B.-O., & Seager, S. 2011, *ApJs*, 197, 12

de Pater, I., Lissauer, J. J., 2001, *Planetary Sciences*, Cambridge University Press, Cambridge, UK

Désert, J.-M., Vidal-Madjar, A., Lecavelier Des Etangs, A., et al. 2008, *A&A*, 492, 585

Désert, J.-M., Sing, D., Vidal-Madjar, A., et al. 2011, *A&A*, 526, A12

Dobbs-Dixon, I., & Lin, D. N. C. 2008, *ApJ*, 673, 513

Eastman, J., Silverd, R., Gaudi, B. S. 2010, *PASP*, 122, 935

Enoch, B., Collier Cameron, A., Parley, N. R., & Hebb, L. 2010, *A&A*, 516, A33

Fortney, J. J., Marley, M. S., Lodders, K., Saumon, D., & Freedman, R. 2005, *ApJ*, 627, L69

Fortney, J. J., Marley, M. S., & Barneset, J. W. 2007, *ApJ*, 659, 1661

Fortney, J. J., Lodders, K., Marley, M. S., & Freedman, R. S. 2008, *ApJ*, 678, 1419

Fortney, J. J., Shabram, M., Showman, A. P., et al. 2010, *ApJ*, 709, 1396

Fossati, L., Haswell, C. A., Froning, C. S., et al. 2010, *ApJ*, 717, L222

Freedman R. S., Marley M. S., Lodders K. 2008, *ApJ*, 174, 513

Gaudi, B. Scott 2005, *ApJ*, 628, 73

Gibson, N. P., Pollacco, D., Simpson, E. K., et al. 2008, *A&A*, 492, 603

Gibson, N. P., Pont, F., Aigrain, S. 2011, *MNRAS*, 411, 2199

Gibson, N. P., Aigrain, S., Pont, F., et al. 2012, *MNRAS*, 422, 53

Gibson, N. P., Aigrain, S., Barstow, J. K., et al. 2012, *MNRAS* accepted, arXiv:1210.7798

Gillon, M., Pont, F., Moutou, C., et al. 2006, *A&A*, 459, 249

Gillon, M., Demory, B.-O., Benneke, B., et al. 2012, *A&A*, 539, A28

Greiner, J., Bornemann, W., Clemens, C., et al. 2008, *PASP*, 120, 405

Gu, P.-G., Bodenheimer, P. H., & Lin, D. N. C. 2004, *ApJ*, 608, 1076

Guillot, T. 2010, *A&A*, 520, A27

Hansen, B. 2008, *ApJ*, 179, 484

Hartman, J. D., Bakos, G. Á., Béky, B., et al. 2012, *AJ*, 144, 139

Hellier, C., Anderson, D. R., Collier Cameron, A., et al. 2012, arXiv:1204.5095

Hilditch, R. W. 2001, *An Introduction to Close Binary Stars*, Cambridge University Press, Cambridge, UK

Holman, M. J., & Murray, N. W. 2005, *Science*, 307, 1288

Hubbard, W. B., Fortney, J. J., Lunine, J. I., et al. 2001, *ApJ*, 560, 413

Ibgui, L., & Burrows, A. 2009, *ApJ*, 700, 1921

Ibgui, L., Burrows, A., & Spiegel, D. S. 2010, *ApJ*, 713, 751

Jackson, B., Greenberg, R., & Barnes, R., et al. 2008, *ApJ*, 681, 1631

Knutson, H. A., Charbonneau, D., Noyes, R. W., Brown, T. M., & Gilliland, R. L. 2007a, *ApJ*, 655, 564

Knutson, H. A., Charbonneau, D., Allen, L. E., et al. 2007b, *Nature*, 447, 183

Laughlin, G., Crismani, M., & Adams, F. C., 2011, *ApJ*, 729, 7

Lecavelier des Etangs, A., Vidal-Madjar, A., Désert, J.-M., & Sing, D. 2008, *A&A*, 485, 865

Lodders, K., & Fegley, B. 2002, *Icarus*, 155, 393

Lubow, S. H., Ida, S. 2010, *Exoplanets*, edited by S. Seager. (University of Arizona Press), p. 347

Mancini, L., Southworth, J., Ciceri, S., et al. 2013, to appear in *A&A*, arXiv: 1212.3701

Mayor, M., and Queloz, D. 1995, *Nature*, 378, 355

Miller, N., Fortney, J. J., & Jackson, B. 2009, *ApJ*, 702, 1413

Miller, N., & Fortney, J. J. 2011, *ApJ*, 736, L29

Miller-Ricci E. & Fortney J. J. 2010, *ApJ*, 716, 74

Nikolov, N., Henning, Th., Koppenhoefer, J., et al. 2012, *A&A*, 539, 159

Penev, K., Bakos, G. Á., Bayliss, D., et al. 2013, *AJ*, 145, 5

Pollack J. B., Hubickyj O., Bodenheimer P., & Lissauer, J. J. 1996, *Icarus*, 124, 62

Pont, F., Zucker, S., & Queloz, D. 2006, *MNRAS*, 373, 231

Pont, F., Knutson, H., Gilliland, R. L., Moutou, C., & Charbonneau, D. 2008, *MNRAS*, 385, 109

Redfield, S., Endl, M., Cochran, W. D., & Koesterke, L. 2008, *ApJ*, 673, L87

Richardson, L. J., Harrington, J., Seager, S., & Deming, D. 2006, *ApJ*, 649, 1043

Richardson, L. J., Deming, D., Horning, K., Seager, S. & Harrington, J. 2007, *Nature*, 445, 892

Rogers, J. C., Apai, D., López-Morales, M., Sing D. K., & Burrows A. 2009, *ApJ*, 707, 1707

Rothman, L. S., Gordon, I. E., Barber, R. J., et al. 2010, *JQSRT*, 111, 2139

Rowe, J. F., Matthews, J. M., Seager, S., et al. 2006, *ApJ*, 646, 1241

Rowe, J. F., Matthews, J. M., Seager, S., et al. 2008, *ApJ*, 689, 1345

Russell, H. N. 1948, *Harvard Observatory Monographs*, 7, 181

Seager, S., & Sasselov, D. D. 2000, *ApJ*, 537, 916

Seager, S. & Mallén-Ornelas, G. 2003, *ApJ*, 585, 1038

Sing, D. K., Vidal-Madjar, A., Désert, J.-M., Lecavelier des Etangs, A., & Ballester, G. 2008a, *ApJ*, 686, 658

Sing, D. K., Vidal-Madjar, A., Lecavelier des Etangs, A., Désert, J.-M., Ballester, G., & Ehrenreich, D. 2008b, *ApJ*, 686, 667

Sing, D. K., Pont, F., Aigrain, S., et al. 2011a, *MNRAS*, 416, 1443

Sing, D. K., Désert, J.-M., Fortney, J. J., et al. 2011b, *A&A*, 527, A73

Sing, D. K., Huitson, C. M., Lopez-Morales, M., et al. 2012, *MNRAS*, 426, 1663

Siverd, R. J., Beatty, T. G., Pepper, J., et al. 2012, *arXiv:1206.1635*

Smalley, B., Anderson, D. R., Collier-Cameron, A., et al. 2012, *arXiv:1206.1177*

Snellen, I. A. G., Albrecht, S., de Mooij, E. J. W., & Le Poole, R. S. 2008, *A&A*, 487, 357

Snellen, I. A. G., de Kok, R. J., de Mooij, E. J. W., & Albrecht, S. 2010, *Nature*, 465, 1049

Southworth, J. 2008, *MNRAS*, 386, 1644

Southworth, J. 2009, *MNRAS*, 394, 272

Southworth, J. 2010, *MNRAS*, 408, 1689

Southworth, J. 2011, *MNRAS*, 417, 2166

Southworth, J. 2012, *MNRAS*, 426, 1291

Southworth, J., Maxted, P. F. L., Smalley, B., 2005, *A&A*, 429, 645

Southworth, J., Wheatley P. J., Sams G., 2007, *MNRAS*, 379, L11

Southworth, J., Hinse, T. C., Jørgensen, U. G., et al., 2009, *MNRAS*, 396, 1023

Southworth, J., Bruni, I., Mancini, L., J. Gregorio 2012a, *MNRAS* 420, 2580

Southworth, J., Mancini, L., Maxted, P. F. L., et al. 2012b, *MNRAS*, 422, 3099

Spiegel, D. S., Silverio, K., Burrows, A. 2009, *ApJ*, 699, 1487

Stetson, P. B., 1987, *PASP*, 99, 191

Sudarsky D., Burrows A., Pinto P. 2000, *ApJ*, 538, 885

Sudarsky, D., Burrows, A., & Pinto, P. 2000, *ApJ*, 538, 885

Sudarsky, D., Burrows, A., & Hubeny, I. 2003, *ApJ*, 588, 1121

Swain, M. R., Vasisht, G., & Tinetti, G. 2008, *Nature*, 452, 329

Tinetti, G., Vidal-Madjar, A., Liang, M.-C., et al. 2007, *Nature*, 448, 169

Tinetti, G., Deroo, P., Swain, M. R., et al. 2010, *ApJ*, 712, L129

Vidal-Madjar, A., et al. 2003, *Nature*, 422, 143

Vidal-Madjar, A., Désert, J.-M., Lecavelier des Etangs, A., et al. 2004, *ApJ*, 604, L69

Winn, J. N., Noyes, R. W., Holman, M. J., et al. 2005, *ApJ*, 631, 1215

Winn, J. N., Holman, M. J., Bakos, G. Á., et al. 2007, *AJ*, 134, 1707

Winn, J. N., Holman, M. J., Torres, G., et al. 2008, *ApJ*, 683, 1076

Winn, J. N., Holman, M. J., Carter, J. A., et al. 2009, *AJ*, 137, 3826

Wood, P. L., Maxted, P. F. L., Smalley, B., Iro, N. 2011, *MNRAS*, 412, 2376

Zahnle, K., Marley, M. S., Freedman, R. S., Lodders, K., & Fortney, J. J. 2009, *ApJ*, 701, L20

APPENDIX A: GROND-NIR DATA REDUCTION

The calibration of the GROND NIR data is a little more complicated than the optical data, because of the presence of electronic odd-even read-out pattern along the y-axis. In order to remove this pattern, we smooth each image and compare it with the unsmoothed ones after the master dark has been subtracted. The amplitudes of the read-out pattern are then determined by comparing the median level of each column to the overall median level. Each column is shifted back to the overall median level. The master skyflats are divided out from the science images after the removal of read-out pattern.

Since our observations are in staring mode, sky background is an important contribution in the images. With the 20-position dithering sky measurements right before and after the science time series, we could construct a sky emission model for each science image. These sky images are calibrated in the same way as the science images. We mask out all the stars in the calibrated sky images, and normalise each image with their own overall median levels. All the normalised skies are then median combined, and normalised again. For each science image, we scale the pre- and post-science sky models to their background individually. The final sky model is constructed by weighted combining them according to the inverse square of fitted χ^2 . This sky model is then subtracted from corresponding science image. After

sky subtraction, we still see remnant structure, which is expected due to the variation of the sky during the observing sequence.

After these calibrations have been applied, we perform aperture photometry on WASP-44 as well as three nearby comparison stars. The locations of each star are determined by IDL/FIND, which calculates the centroids by fitting Gaussians to the marginal x and y distributions. In order to find the optimal photometry, we lay 30 apertures on all the stars in step of 0.5 pixel, each with ten annuli in step of 1 pixel. This produces 300 datasets with different aperture settings. In this way, the above mentioned sky subtraction remnant effect is accounted for in the sky annulus adopted in the aperture photometry. We divide the flux of each star with its own median value. A composite reference light curve is constructed by median-combining fluxes of ensembles of comparison stars, which are required to show the least deviation from the target. We normalize the target light curve with this composite reference light curve.

Since the normalised light curve still shows strong red noise correlated with positions, seeing and airmass, instead of selecting the optimal photometry directly from *rms* of out-of-transit baseline, we fit the whole light curve simultaneously with the theoretical light curve model multiplied with a baseline correction function. This correction function consists of positions/time in quadratic form, and FWHMs/airmass in linear form. We tried to select the optimal light curves by choosing the ones with the least *rms* of O–C flux residuals among all the datasets. However, the transit depths of the optimal light curves of the same band from different nights are very deviant from each other. We note that light curves of the same band obtained using different aperture and annulus sizes could exhibit similar least *rms*, however produce different transit depths. Therefore, for each NIR band, we choose the two light curves with the least *rms* and with consistent transit depth between the two nights as our final optimal photometric results.